Computational and Structural Biotechnology Journal 21 (2023) 5285–5295

Contents lists available at ScienceDirect

Computational and Structural Biotechnology Journal

journal homepage: www.elsevier.com/locate/csbj

Research article

Multiscale modeling of drug resistance in glioblastoma with gene mutations and angiogenesis

Heng Yang [a,b], Haofeng Lin [a,b], Xiaoqiang Sun [b,*]

[a] Zhongshan School of Medicine, Sun Yat-Sen University, Guangzhou 510080, China
[b] School of Mathematics, Sun Yat-Sen University, Guangzhou 510275, China

ARTICLE INFO

Keywords:
Multiscale modeling
Genetic mutations
Angiogenesis
Drug resistance

ABSTRACT

Drug resistance is a prominent impediment to the efficacy of targeted therapies across various cancer types, including glioblastoma (GBM). However, comprehending the intricate intracellular and extracellular mechanisms underlying drug resistance remains elusive. Empirical investigations have elucidated that genetic aberrations, such as gene mutations, along with microenvironmental adaptation, notably angiogenesis, act as pivotal drivers of tumor progression and drug resistance. Nonetheless, mathematical models frequently compartmentalize these factors in isolation. In this study, we present a multiscale agent-based model of GBM, encompassing cellular dynamics, intricate signaling pathways, gene mutations, angiogenesis, and therapeutic interventions. This integrative framework facilitates an exploration of the interplay between genetic mutations and the vascular microenvironment in shaping the dynamic evolution of tumors during treatment with tyrosine kinase inhibitor. Our simulations unveil that mutations influencing the migration and proliferation of tumor cells expedite the emergence of phenotype heterogeneity, thereby exacerbating tumor invasion under both treated and untreated conditions. Moreover, angiogenesis proximate to the tumor fosters a protumoral milieu, augmenting mutation-induced drug resistance by increasing the survival rate of tumor cells. Collectively, our findings underscore the dual roles of intrinsic genetic mutations and extrinsic microenvironmental adaptations in steering tumor growth and drug resistance. Finally, we substantiate our model predictions concerning the impact of gene mutations and angiogenesis on the responsiveness of targeted therapies by integrating single-cell RNA-seq, spatial transcriptomics, bulk RNA-seq, and clinical data from GBM patients. The multidimensional approach enhances our understanding of the complexities governing drug resistance in glioma and offers insights into potential therapeutic strategies.

1. Introduction

As a type of primary brain tumor, glioblastoma (GBM) is one of the most malignant cancers [1]. Many previous studies have demonstrated that receptor tyrosine kinase (RTK) signaling pathways are often highly activated in most GBM tumors [2]. Multiple RTK inhibitors, including tyrosine kinase inhibitors (TKIs), are being developed and evaluated in clinical trials. However, most of the TKI therapies for GBM show limited efficacy in clinical Phase II/III trials [3]. The formidable challenge of TKI resistance looms large, significantly limiting the clinical effectiveness of targeted therapies in GBMs. While experimental studies have yielded invaluable insights into various facets of drug resistance mechanisms, a comprehensive and systematic understanding of these intricate mechanisms remains elusive, posing a substantial impediment to progress in the field of tumor treatment.

Drug resistance in tumor can manifest either as an inherent trait (referred to as intrinsic resistance) or as an adaptive response that develops subsequent to a period of drug therapy (known as acquired resistance). Traditional investigations into the mechanisms of drug resistance have mainly focused on tumor cells themselves, encompassing inquiries into genetic heterogeneity [4], gene mutations, and epigenetic variations [5]. However, the rapid emergence of acquired resistance remains inadequately accounted for by genetic mutations alone [6,7]. Recent experimental evidence underscores the pivotal role played by the tumor microenvironment in influencing the response to drug therapy [8,9]. Tumor cells cooperate with neighboring cells to create an environment conducive to evading treatment, a phenomenon known as tumor microenvironment-mediated drug resistance [10]. This

* Corresponding author.
E-mail address: sunxq6@mail.sysu.edu.cn (X. Sun).

https://doi.org/10.1016/j.csbj.2023.10.037
Received 21 August 2023; Received in revised form 17 October 2023; Accepted 17 October 2023
Available online 21 October 2023

milieu encompasses the external surroundings within which tumor cells thrive, comprising a diverse array of cell types (e.g., fibroblasts, endothelial cells, and immune cells) and bioactive molecules (e.g., cytokines, growth factors, and chemokines) [9].

Theoretical modeling of tumor drug resistance presents a formidable challenge [11], spurring researchers to explore diverse methods and perspectives. Tumor cell populations are inherently heterogeneous, consisting of both drug-sensitive and drug-resistant cells. Historically, mathematical models have been developed at the cellular population level to elucidate the dynamics of tumor drug resistance. For instance, Panetta et al. [12] formulated a mathematical model comprising two ordinary differential equations (ODEs) to describe the growth and evolution of heterogeneous tumor cell populations (drug-sensitive and drug-resistant) during chemotherapy. This model was instrumental in the analysis of effective treatment options and the optimization of drug combinations to enhance therapeutic outcomes. Foo et al. [13] established a stochastic model to investigate the evolutionary kinetics of tumor cell populations (drug-sensitive and drug-resistant) and to delineate strategies for optimizing drug dosages during treatment. Subsequently, Pisco et al. [14] introduced the Markov state transition model and ODE model, employing an integrative experimental and modeling approach to explore the influence of cell growth rates and phenotypic transition rates on cell population homeostasis. Their work explained the emergence of multi-drug resistance in drug-treated leukemia cancer cells. Furthermore, Nowak et al. applied branching process models to study the temporal evolution of gene mutations associated with intrinsic resistance [15] and resistance resulting from spatial heterogeneity in drug concentrations [16]. Nevertheless, few existing models integrate gene mutations and the vascular microenvironment to scrutinize their collective impact on drug resistance.

Building upon the foundation of our prior investigations [17,18], the present study advances a multiscale model of drug resistance. This model integrates an agent-based representation of cellular phenotypes, ODEs of signaling pathways, stochastic simulations of gene mutations, spatial–temporal evolutions of microenvironmental factors, and rule-based simulations of angiogenesis. Within this framework, we investigated the ramifications of mutation timings and distance from the parent vessels to the tumor on the efficacy of drug treatment. Furthermore, we delved into the underlying mechanisms governing cellular heterogeneity and microenvironmental adaptations, both of which influence the spatial–temporal dynamics of tumor growth and drug resistance. Lastly, we substantiated our model predictions by using single-cell RNA-seq, spatial transcriptomics, bulk RNA-seq, and clinical data to perform survival analysis among glioma patients undergoing targeted therapies.

2. Mathematical modeling and simulation

We described a multiscale agent-based model for GBM, encompassing microenvironmental factors, signaling pathways, cellular agents bearing gene mutations, angiogenesis, and drug treatment. This model operates across three scales: microenvironmental scale, molecular scale, and cellular scale. At microenvironmental scale, we consider five microenvironmental factors (i.e., glucose, oxygen, epidermal growth factor (EGF), vascular endothelial growth factor (VEGF), and fibronectin) as well as drug (e.g., TKI); at molecular scale, we consider EGFR signaling pathway and cell cycle pathway; at cellular scale, we consider cell agents, gene mutations, and angiogenesis. Of note, as signaling mechanisms underlying tumor cell-microenvironment are complicated, we used EGF as a representative growth factor in the tumor microenvironment and a classical epidermal growth factor receptor (EGFR) pathway as a representative oncogenic signaling pathway, since EGFR is one of the most-altered RTKs in GBM [2].

To characterize the spatial-temporal dynamics of microenvironmental factors and drugs diffusion, production, and/or degradation, we employed a lattice-based spatial–temporal discrete model. The intracellular EGFR signaling pathways targeted by an EGFR-targeting TKI were simulated through ODEs based on the law of mass action and Michalis-Menten kinetics. The diverse phenotypes of tumor cells were accounted for by postulating that gene mutations affect parameters governing cell migration and proliferation. The behavior of tumor cells was simulated using an agent-based model. Additionally, the generation and expansion of new blood vessels (i.e., angiogenesis), which profoundly reshapes the microenvironment, were also integrated into our model at the cellular scale.

The simulation was conducted within a 200×200 two-dimensional lattice, where each grid element represented a spatial resolution of $20\mu m$, approximating the diameter of individual tumor cells. A single cell occupied only one grid. Initially, a parent vessel along with six vascular buds was situated at the bottom boundary of the lattice, while several tumor cells were randomly distributed near the center of the lattice.

2.1. Microenvironmental scale

The microenvironment provides tumor cells with a conducive space for survival and a source of nutrients. It also serves as a bridge connecting angiogenesis with tumor cells. Six key continuous variables are implicated in the microenvironmental scale: glucose concentration (G), oxygen concentration (O), fibronectin concentration (N), EGF concentration (E), VEGF concentration (V), and drug concentration (D). Each variable (X) may undergo processes of penetration, diffusion, uptake, or decay. Generally, these processes can be summarized by the following equation:

$$\frac{X_{i,j}^{l+1}-X_{i,j}^{l}}{\Delta t}=\overbrace{d_X\nabla^2 X_{i,j}^{l}}^{difussion}+\overbrace{p_X(X^{blood}-X_{i,j}^{l})\chi_1(l,i,j)}^{vessel\ penetration}+\overbrace{v_X\chi_1(l,i,j)}^{vessel\ secretion}+\overbrace{s_X\chi_2(l,i,j)}^{tumor\ secretion}-\overbrace{u_X\chi_2(l,i,j)}^{tumor\ uptake}-\overbrace{\delta_X X_{i,j}^{l}}^{decay} \tag{1}$$

where $\nabla^2 X_{i,j}^{l}=\frac{X_{i+1,j}^{l}+X_{i-1,j}^{l}+X_{i,j+1}^{l}+X_{i,j-1}^{l}-4X_{i,j}^{l}}{h^2}$ and h is the mesh size. Δt is the timestep used for updating the concentration of microenvironmental factors, which is set to 1 second in this study. d_X stands for the diffusion coefficient of X. p_X is the vessel penetration rate of X. X^{blood} signifies the X concentration within the blood vessel. v_X, s_X, u_X, and δ_X are the vessel secretion, tumor secretion, tumor uptake, and natural decay rates of X, respectively. We define $\chi_1(l,i,j)=1$when a vessel cell is present at the position (i,j) in the l-th iteration; otherwise, $\chi_1(l,i,j)=0$. Similarly, we set $\chi_2(l,i,j)=1$ when the position (i,j) is occupied by a tumor cell in the l-th iteration; otherwise, $\chi_2(l,i,j)=0$. To ensure non-negativity of concentrations, we apply $X_{i,j}^{l+1}=\max(0,X_{i,j}^{l+1})$ in each iteration. The specific equation for each variable is described below.

Glucose, oxygen, and EGF each play crucial roles in tumor growth. Glucose supplies essential nutrients for cellular activity, while oxygen impacts signaling components in the cell cycle pathway. EGF, on the other hand, represents a ligand secreted by tumor cells that binds to EGFR, thereby initiating an autocrine signaling pathway.. Their evolutions can be described by the following reaction-diffusion equations:

$$\frac{G_{i,j}^{l+1}-G_{i,j}^{l}}{\Delta t}=d_G\nabla^2 G_{i,j}^{l}+p_G\left(G^{blood}-G_{i,j}^{l}\right)\chi_1(l,i,j)-u_G\chi_2(l,i,j), \tag{2}$$

$$\frac{O_{i,j}^{l+1}-O_{i,j}^{l}}{\Delta t}=d_O\nabla^2 O_{i,j}^{l}+p_O\left(O^{blood}-O_{i,j}^{l}\right)\chi_1(l,i,j)-u_O\chi_2(l,i,j), \tag{3}$$

$$\frac{E_{i,j}^{l+1}-E_{i,j}^{l}}{\Delta t}=d_E\nabla^2 E_{i,j}^{l}+s_E\chi_2(l,i,j)-\delta_E E_{i,j}^{l}. \tag{4}$$

VEGF and fibronectin exert influence over angiogenesis. VEGF is secreted by hypoxic tumor cells to stimulate blood cell growth, and is consumed by endothelial cells [19]. Conversely, fibronectin, acting as a

haptotaxis factor for endothelial cells, is secreted by the endothelial cells and can be absorbed by invasive tumor cells. We describe their evolutions by the following equations:

$$\frac{V_{i,j}^{l+1} - V_{i,j}^{l}}{\Delta t} = d_V \nabla^2 V_{i,j}^{l} - \quad \chi_1(l,i,j) p_V V_{i,j}^{l} + s_V \chi_2(l,i,j) - \delta_V V_{i,j}^{l}, \tag{5}$$

$$\frac{N_{i,j}^{l+1} - N_{i,j}^{l}}{\Delta t} = v_N \chi_1(l,i,j) - \chi_2(l,i,j) u_N N_{i,j}^{l}. \tag{6}$$

TKIs are considered as EGFR inhibitor in this study. They exert their inhibitory effects on tumor progression by binding to EGFR, thereby modulating cellular functions (e.g., migration and proliferation) through the EGFR signaling pathway. The drug is delivered and

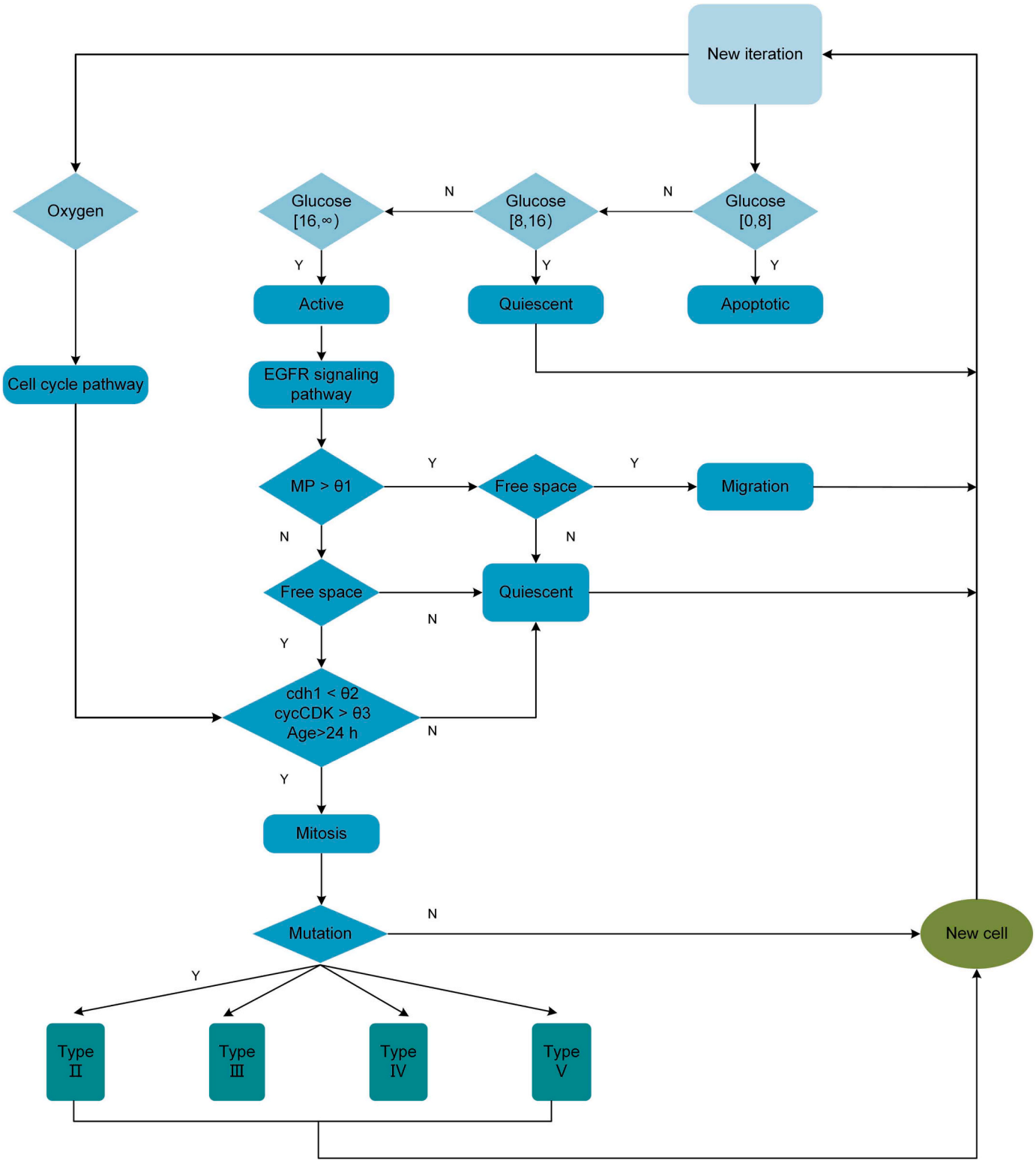

Fig. 1. Flowchart of cell fate determination. Abbreviations: MP, migration potential; cdh1, Cadherin 1; cycCDK, Cyclin-dependent Kinase;.

permeated via blood vessels and diffuses across the microenvironment, as described in the following equation:

$$\frac{D_{i,j}^{l+1} - D_{i,j}^{l}}{\Delta t} = d_D \nabla^2 D_{i,j}^{l} + p_D \left(D^{blood} - D_{i,j}^{l} \right) \chi_1(l,i,j) - u_D \chi_2(l,i,j) - \delta_D D_{i,j}^{l}. \tag{7}$$

The homogeneous Neumann boundary conditions are applied for the abovementioned equations by assuming zero flux along the boundary of the domain.

2.2. Molecular scale

At the molecular scale, we scrutinized the EGFR signaling pathway and the cell-cycle pathway for each tumor cell. EGFR activation ensued upon EGF ligand binding, subsequently propagating downstream signals and inciting the cell-cycle pathway. The EGFR signaling pathway [20,21] considered in this study is illustrated in Fig. A.1.

Treatment with TKIs impeded EGFR activation. Assuming rapid binding and unbinding kinetics between EGFR and TKI, we modeled the EGFR:TKI complex (R:D) utilizing the following Hill equation based on Michaelis–Menten kinetics:

$$[R:D] = \frac{[R]_0 \bullet [D]}{k_m + [D]},$$

where k_m is the Michaelis constant and $[R]_0$ is the initial concentration of EGFR. Thus, the quantity of effective EGFR is derived as follows:

$$[R]_{eff} = [R]_0 - [R:D]. \tag{8}$$

Based on the law of mass action, the biochemical reactions among the molecular species in these pathways are described by the ODEs:

$$\frac{dx_i}{dt} = f(x), \tag{9}$$

where $f(x) = \sum v_+ - \sum v_-$, with v_+ and v_- representing the production and consumption rates of substance x_i, respectively. The details of ODEs are listed in **Appendix B**.

2.3. Cellular scale

2.3.1. Agent-based model of cell behaviors

At the cellular scale, each tumor cell is viewed as an individual agent. It receives signals from the microenvironment and dynamically adjusts its behavior in response, following the rules below (Fig. 1):

1. Initially, each cell chooses one of the following states: active, quiescent (reversible), or apoptotic (irreversible), depending on the glucose concentration at its location and the neighboring space. Only active cells can migrate or proliferate based on the state of the signaling pathway.
2. Each active cell assesses its migration potential $MP = \frac{\Delta[PLC_\gamma]}{\Delta t}$ to determine whether migration is possible. If $MP > \theta_1$, the cell migrates, where θ_1 is a threshold set to be the average change rate of PLC_γ. In such instances, each cell chooses the most favorable surrounding vacant space according to the following score:

$$S_{ij} = \frac{\alpha G_{ij}}{N_{ij}} + (1-\alpha)\varepsilon_{ij}, \tag{10}$$

where G_{ij} and N_{ij} represent the concentrations of glucose and fibronectin at position (i,j), respectively. $\varepsilon_{ij} \sim N(0,1)$ denotes an error term following a normal distribution, while α stands for the search precision and is set to 0.7 [22].
3. Otherwise, if $MP < \theta_1$, the cell does not migrate and evaluates activities of *cdh*1 and *cycCDK* in the cell cycle pathway to determine its potential for proliferation. If $[cdh1] < \theta_2$, $[cycCDK] > \theta_3$, and the age of the tumor cell is > 24 h, then the cell proliferates and divides into two daughter cells.

2.3.2. Stochastic simulation of gene mutations

We assume that gene mutations affect the migration and proliferation of tumor cells by modulating specific threshold parameters: θ_1, θ_2, and θ_3 (Table 1). Lowering θ_1 augments cell migration potential, whereas elevating θ_2 or reducing θ_3 expedites cellular proliferation (Fig. 1). Consequently, we defined five distinct tumor cell phenotypes characterized by varying migration and proliferation capacities, as outlined in Table 1. Notably, our choice of parameters aligns with established values of $s = 0.05$ and $t = 0.03$ [17,18].

Phenotype I corresponds to the wild-type (WT) tumor cells, while phenotypes II–V represent mutated variants. Cells embodying phenotype II exhibit heightened migratory tendencies compared to WT cells, while those with phenotype III display the converse behavior. Furthermore, phenotype IV or V pertains to tumor cells exhibiting diminished or augmented proliferation capabilities, respectively.

Initially, all tumor cells are presumed non-mutated, reflecting phenotype I. During cell division, there exists a slight probability of mutation ($p_{mutation} = 0.1$). When mutations occur, each of the resultant daughter cells is randomly assigned one of the four mutant phenotypes, with each phenotype holding an equal likelihood of selection. Then, the daughter cells participate in the subsequent simulation iteration, using the newly acquired threshold parameters corresponding to their assigned phenotypes. Of note, the mutant phenotypes can mutate again in the subsequent simulation iteration.

2.3.3. Rule-based simulation of angiogenesis

We also consider the effect of angiogenesis on tumor growth at the cellular scale. We hypothesize that the migration of endothelial cells is guided by chemotaxis toward VEGF and haptotaxis toward fibronectin. Therefore, we defined the migration probability of endothelial cells as follows:

$$\begin{aligned}
P_1 &= \frac{ck_V}{k_V + V(i,j)}(V(i,j+1) - V(i,j)) + \lambda(N(i,j+1) - N(i,j)),\\
P_2 &= \frac{ck_V}{k_V + V(i,j)}(V(i,j-1) - V(i,j)) + \lambda(N(i,j-1) - N(i,j)),\\
P_2 &= \frac{ck_V}{k_V + V(i,j)}(V(i,j-1) - V(i,j)) + \lambda(N(i,j-1) - N(i,j)),\\
P_4 &= \frac{ck_V}{k_V + V(i,j)}(V(i+1,j) - V(i,j)) + \lambda(N(i+1,j) - N(i,j)),\\
P_5 &= \frac{P_1 + P_2 + P_3 + P_4}{4},
\end{aligned} \tag{11}$$

where V represents the concentration of VEGF, while N signifies the concentration of fibronectin. c denotes the chemotaxis coefficient, and k_V controls the weight of VEGF concentration in chemotaxis sensitivity. Additionally, λ is the chemotactic coefficient. The probabilities denoted as P_{1-5} correspond to the likelihoods of endothelial cells moving up, down, left, or right, or remaining stationary, respectively. Moreover, for every sprout tip cell, if the age of the vessel is greater than 18 h and there is free space in its immediate neighborhood, the sprout bifurcates into two vessels.

2.4. Multiscale integration and simulation workflow

To integrate multiple scales in silico, the following computational procedures were performed within each iteration step:

1. At the microenvironment scale: solve Eqs. (2–7) to update the spatial–temporal distributions of glucose, oxygen, fibronectin, EGF, VEGF, and TKI. The timestep for updating the concentrations of microenvironmental factors is set to 1 s.

Table 1
Phenotypes and their random threshold parameters.

Phenotype	I (WT)	II (Migration ↑)	III (Migration ↓)	IV (Proliferation ↓)	V (Proliferation ↑)
$\boldsymbol{\theta_1}$	k	$(0,k)$	$(k,2k)$	k	k
$\boldsymbol{\theta_2}$	s	s	s	$(0,s)$	$(s,2s)$
$\boldsymbol{\theta_3}$	t	t	t	$(t,2t)$	$(0,t)$

2. At the molecular scale: utilize the drug concentration obtained in step 1 to calculate the effective EGFR [Eq. (8)]. Furthermore, employ the computed concentrations of EGF and oxygen as input to solve Eq. (9) for updating the EGFR signaling pathway and cell-cycle pathway.
3. At the cellular scale: subject each tumor cell to migration, proliferation, or mutation in accordance with the predefined rules influenced by microenvironmental factors, neighboring space, and signaling activities. Additionally, angiogenesis is considered at the cellular scale: sprout tip endothelial cells migrate as per Eq. (11) or undergo branching if the age of the vessel is $>$ 18 h. The timestep for updating cell activity is set to 1 h.

Within each iteration step (1 h), the numerical simulations for solving PDEs at microscale (1 s) were continuously updated 3600 times; and at the end of 1 h, the cell activities were updated, which influences the spatial distribution of tumor cells and vessel cells that in turn influence the reaction terms of PDEs. In this way, the microscale and macroscale were coupled.

The model parameters (**Appendix C**) were adapted from our previous works [17,18].

2.5. Survival analysis for verifying model predictions

To verify the prognostic effects of gene mutations and angiogenesis in glioma patients undergoing targeted therapies, we collected single-cell RNA-seq data, bulk RNA-seq data, spatial transcriptomics, clinical profiles, and somatic mutation data for GBM patients. The bulk RNA-seq, clinical information, and somatic mutation records for GBM patients were sourced from the TCGA database (https://cancergenome.nih.gov/). Our analysis encompassed a cohort of 19 GBM patients who had received targeted drug therapy and possessed available gene expression, somatic mutation, and clinical data.

To investigate the prognostic impact of genetic mutations, we quantified the number of genes with somatic mutations for each GBM patient. Employing the ROC method [23], we determined the optimal cutoff value, categorizing the 19 GBM cases into two groups: a "more-mutation" group and a "less-mutation" group. We subsequently conducted Kaplan-Meier (K-M) analysis to analyze the progression-free survival (PFS) among the patient group, with the statistical significance of differences assessed using the two-sided log-rank test.

To verify the prognostic implications of angiogenesis in drug resistance, we performed K-M survival analysis to explore the clinical association of tumor progression with the distance between tumors and blood vessels. To accomplish this, we harnessed bulk2space [24] to deconvolute each of the 19 bulk RNA-seq samples into single-cell resolution data with spatial coordinates, using the single-cell RNA-seq data and spatial transcriptomics data of GBM patients as references for deconvolution. The single-cell RNA-seq data [25] were downloaded from the GEO database (GSE182109), while spatial transcriptomic data [26] were retrieved from https://github.com/theMILOlab/SPATAData with sample ID #243UKF. Based on the deconvoluted data, we computed the distance matrix between glioma cells and endothelial cells within each bulk RNA-seq sample. For K-M survival analysis, the 19 patients were divided into a "close" and a "far" group according to the mean value of the distance matrix.

Finally, we examined whether combined variables, encompassing gene mutation numbers and vessel-tumor distance, carried superior prognostic significance compared to individual variables. We built a multivariable Cox regression model based on two binary variables, gene mutation numbers (more $=1$, less $=2$) and tumor-vessel distance (far $=1$, close $=2$), to calculate a risk score for each glioma patient. Risk score $=\sum_{i=1}^{2}\beta_i \times x_i$, where β_i is the regression coefficient and x_i denotes the value of each variable. Patients were divided into a high-risk and low-risk score groups based on the optimal cutoff value of the risk score. K-M analysis for PFS was subsequently conducted for both groups, with statistical significance was assessed using the two-sided log-rank test.

3. Results

3.1. The model recapitulates evolutionary dynamics of vascular tumor growth with gene mutations

We first examined the effects of mutation timings on the spatial–temporal dynamics of tumor growth in the absence of TKI treatment. In order to bolster the robustness of our findings, we performed a total of 10 separate simulations. Within these simulations, tumors initiated mutation at time points of 0, 50, or 100 h, persisting in growth for a duration of 150 h. We recorded the temporal alterations in the tumor cell counts across these 10 simulations, in addition to capturing the spatial distribution of tumors at the conclusion of the first simulation (Fig. 2).

Fig. 2a shows that tumors originating from mutations at 0 h exhibit a greater cell count than unmutated tumors, indicating the capacity of genetic mutations to propel malignant tumor expansion. In addition, the number of tumor cells arising from mutations at 0 h significantly surpasses those originating from mutations at 100 h, implying that the earlier the mutation occurs, the more tumor growth can be promoted. Fig. 2b-e portray the spatial distribution of tumors at the 150-hour mark under various mutation scenarios. These depictions consistently reveal that migrating and proliferating cells predominantly occupy the outermost tumor layer, while apoptotic or quiescent cells are predominantly nestled within. This observation suggests that the outer layer of the tumor benefits from a more abundant living environment and nutrients supply compared to the inner regions.

Given the close association between the defined mutant phenotypes and the proliferation and migration capabilities of tumor cells, we delved into determining which ability predominantly fosters tumor progression. Thus, we monitored the cell counts and phenotype distributions within tumors across different mutational scenarios (Fig. 3).

Fig. 3a–c indicate that, despite the coexistence of all phenotypes, phenotypes I and II dominate the tumor cell population, each forming distinct colonies. Phenotype I represents the wild type, while phenotype II promotes tumor cell migration, suggesting that an enhancement in the migratory capacity of tumor cells may expedite malignant tumor growth. As shown in Fig. 2b–e, numerous cells within the tumor assume a quiescent or apoptotic state due to their incapacity to move or the scarcity of nutrients, while active cells near the tumor boundary enjoy ample space and resource availability. Hence, it is reasonable to speculate that elevating the migration ability of tumor cells affords them more living space and resources, thereby elucidating the prominence of phenotype II.

In addition, we conducted simulations involving deterministic threshold parameters (θ_1, θ_2, and θ_3) associated with gene mutations (Appendix E). Fig. E.1 and Fig. E.2 present findings consistent with the aforementioned observations, reinforcing the tumor-promoting effect of

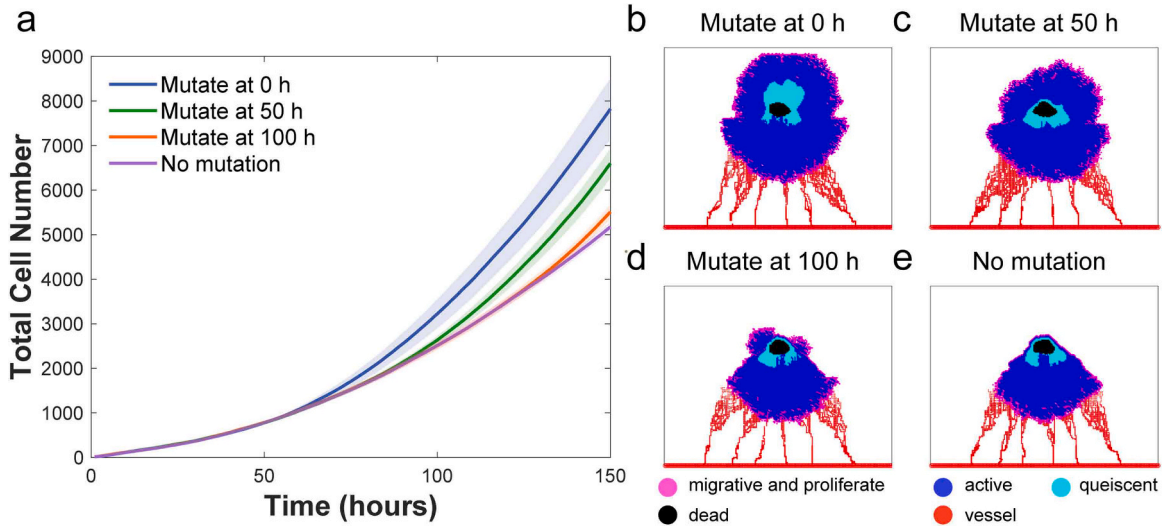

Fig. 2. Evolutionary dynamics of vascular tumor growth with gene mutations. (a) Temporal evolution of tumor cell numbers across ten simulations with varied mutation timing. The lines represent the mean tumor cell numbers, while the shaded areas show the 95% confidence intervals. (b–e) Spatial patterns of the vascular tumor growth in the first simulation (evaluated at 150 h), with gene mutations commencing at 0 h (b), 50 h (c), and 100 h (d), as well as no mutations (e). Different colors indicate various cell types or cellular states: vascular cells (red), proliferating or migrating tumor cells (magenta), active tumor cells (blue), quiescent tumor cells (cyan), and dead tumor cells (black).

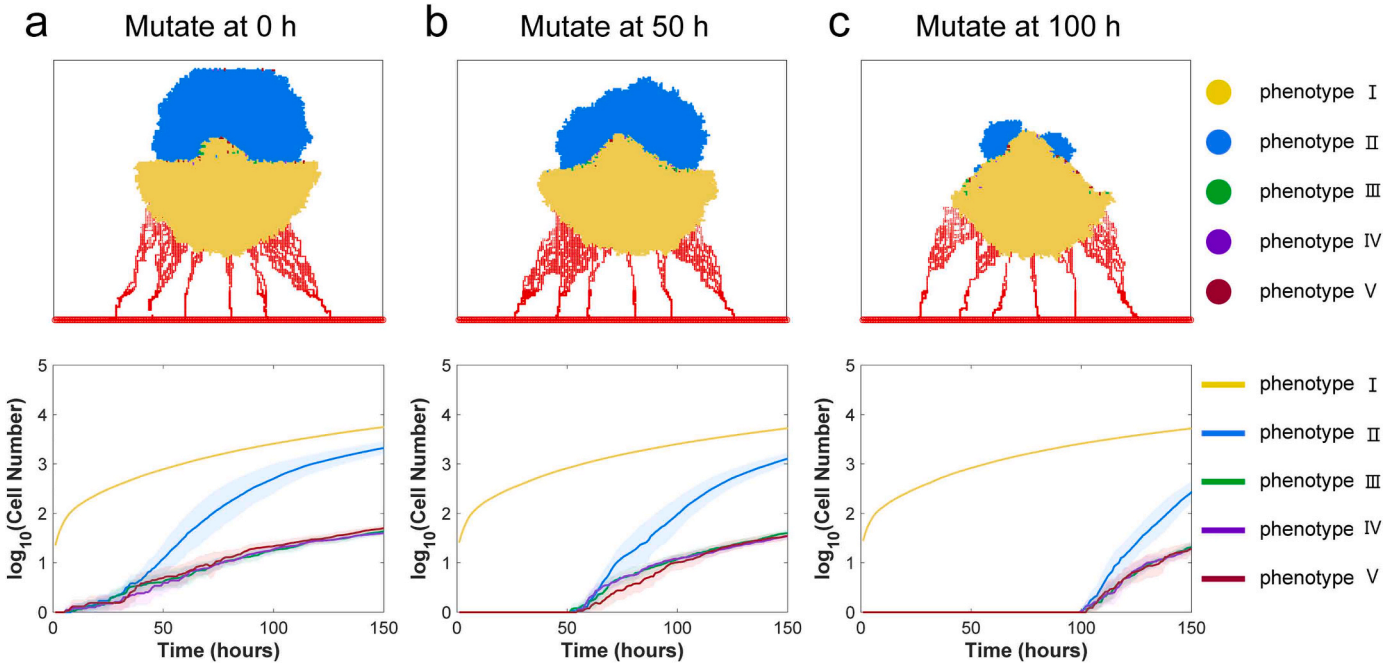

Fig. 3. Spatial distribution and temporal dynamics of a heterogeneous cell population in the absence of drug treatment. Vascular tumor growth with five different phenotypes of tumor cells, each initiated at different mutation timings, was examined. (a) Mutation commencing at 0 h; (b) Mutations commencing at 50 h; (c) Mutations commencing at 100 h. In the lower panel, solid lines represent the mean values of $\log_{10}$(cell number), while shaded areas indicate the 95% confidence intervals.

phenotypic heterogeneity stemming from gene mutations in the context of cancer progression.

3.2. Impact of gene mutations on drug efficacy

In the simulation, we treated tumors with TKIs, which bind to EGFR and consequently diminish the cell migration potential (Fig. 1). A total of 10 simulations were performed to enhance the robustness of the findings. In these simulations, tumors started to mutate at time points of 0, 50, or 100 h. Fig. 4 shows the various vascular tumor growth patterns under different conditions of mutation timings.

Compared to untreated cases, TKI treatment significantly slowed down tumor growth, indicating its inhibitory prowess against tumor expansion. We also observed that gene mutations exerted a pronounced reduction in treatment effectiveness. Notably, tumors harboring earlier mutations manifested amplified tumor cell counts (Fig. 4**a**) and a heightened proportion of migratory and proliferative tumor cells (Fig. 4**b**). These results accentuate the role of gene mutations within tumor cells enhancing their drug resistance.

To investigate the most viable tumor cell phenotypes during drug

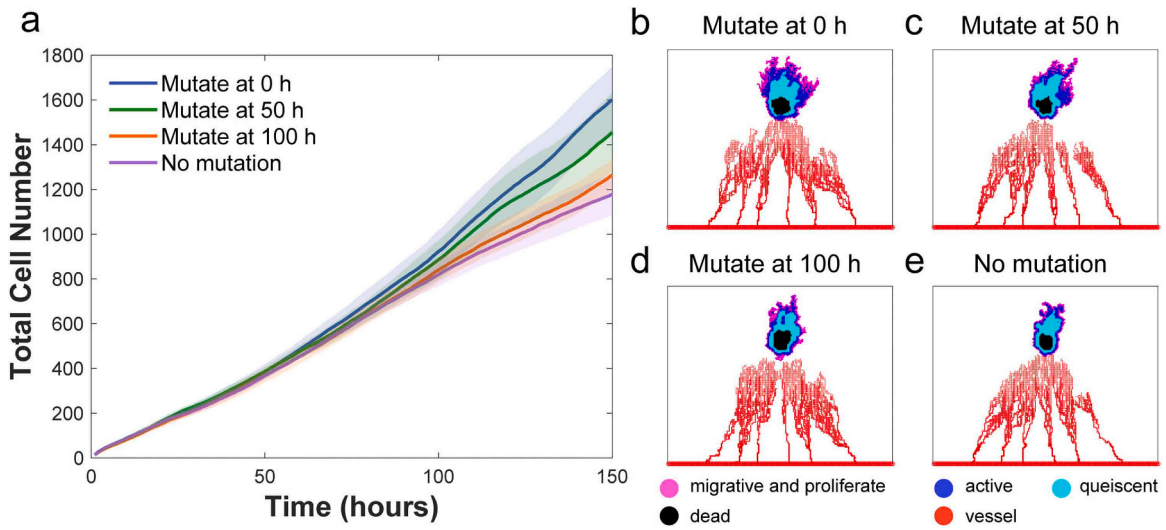

Fig. 4. Tumor growth dynamics with TKI treatment. (a) Temporal changes in the number of tumor cells under varying mutation timings, based on the results of ten simulations. The lines represent the mean tumor cell counts, while the shaded areas show the 95% confidence intervals. (b–e) Spatial patterns of vascular tumor growth in the first simulation (evaluated at 150 h) with gene mutations starting at different time points: 0 h (b), 50 h (c), and 100 h (d), as well as no mutations (e). Different colors denote distinct cell types or states: vascular cells (red), proliferating or migrating tumor cells (magenta), active tumor cells (blue), quiescent tumor cells (cyan), and dead tumor cells (black).

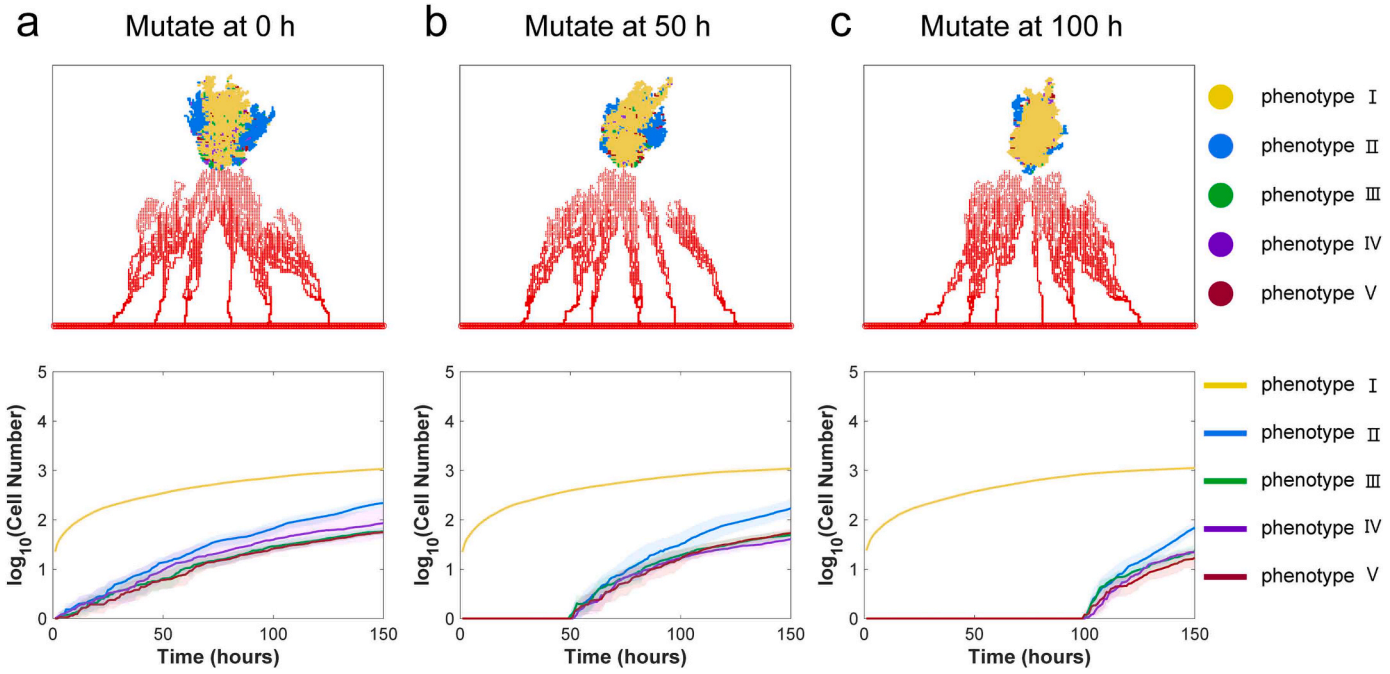

Fig. 5. Spatial distribution and temporal dynamics of heterogeneous tumor cells with TKI treatment. The vascular tumor growth, characterized by five different phenotypes of tumor cells, was examined under various mutation initiation times. (a) Mutation initiation at 0 h; (b) Mutation initiation at 50 h; (c) Mutation initiation at 100 h. In the lower panel, solid lines represent the mean value of $\log_{10}(\text{cell numbers})$, while shaded areas indicate the 95% confidence intervals.

treatment, we scrutinized the evolution and distribution of different phenotypes within the diverse mutation timings scenarios (Fig. 5). It is evident that among the heterogeneous cell populations, phenotype II tumor cells have a survival advantage over other mutant phenotypes, mirroring the untreated situation. Moreover, earlier mutations resulted in a higher proportion of phenotype II tumor cells surrounding the outer layer of the tumor, thereby promoting tumor expansion and invasion. These results imply that mutations increase the migratory capacity of the tumor cells, potentially facilitating their adaptation to the cytotoxic microenvironment and resistance to drug pressure.

In addition, we conducted simulations using deterministic threshold parameters (θ_1, θ_2, and θ_3) associated with gene mutations (Appendix E). Fig. E.3 and Fig. E.4 consistently affirm the aforementioned observations on the role of gene mutations in accelerating the emergence of acquired drug resistance.

3.3. Impact of vascular microenvironment on tumor progression

Many studies have revealed the pivotal role of angiogenesis in tumor growth and metastasis [27,28]. The vascular microenvironment serves as a conduit for delivering nutrients and growth factors (e.g., glucose, oxygen, and EGF) to support tumor growth while facilitating drug

transport for tumor cell eradication. Tumor cells secrete VEGF, stimulating the growth of blood vessels toward tumors. In our multiscale model, we incorporated the spatial–temporal evolutions of microenvironmental factors to capture the intricate feedback dynamics between tumors and the vascular network. In this context, we investigated the impact of the distance between blood vessels and tumors on tumor growth under drug treatment.

We set five incremental values (0.6, 0.65, 0.7, 0.75, and 0.8) representing the initial distance from the parent blood vessel to the tumor center. These dimensionless values are the proportions of the domain size. Continuous drug treatment was administered to the tumor via vessels, with each scenario examined 10 times. The survival rates of tumor cells () across five scenarios were calculated for comparison (Fig. 6).

The results unveil a clear escalation in the number of tumor cells as the distance between blood vessels and the tumor diminishes (Fig. 6a). This observation indicates that closer vascular proximity confers heightened resistance upon tumor cells against drug treatment. Corroboratively, the survival rate of tumor cells registers a parallel increase as the distance between vessels and tumors shrinks (Fig. 6b), suggesting that closer vessels adjacency affords tumor cells an enhanced supply of nutrients and growth factors, sustaining their viability even amidst drug treatment (Fig. 6c).

3.4. Impact of the vascular microenvironment on mutation-induced drug resistance

After examining the individual effects of gene mutations and the vascular microenvironment on drug efficacy, we investigated the collective impact of these factors on tumor evolution during drug treatment. We applied the rules governing the simulation of mutation-induced phenotypes (Table 1 and Fig. 1). In each simulation, tumors were allowed to grow for 200 h, with mutations commencing at either 0 or 100 h, while considering five vessel-tumor distances (0.6, 0.65, 0.7, 0.75, and 0.8). Each simulation was iterated independently 10 times.

Fig. 7a shows a comparative analysis of tumor cell numbers across various combinations of mutation timing and vessel-tumor distance. The results reveal that tumors characterized by earlier mutations and closer vessel-tumor distances exhibited heightened growth, thus manifesting increased resistance to drug treatment. Fig. 7b–f present the spatial patterns of vascular tumor growth when gene mutations commences at 0 h, in conjunction with varying V-T distances. We observed that tumors closer to the vessels (e.g., V-T distance = 0.6) exhibited a greater prevalence of active cells in the vicinity of vessels and fewer apoptotic cells. These findings indicate that angiogenesis closer to the tumor provides a more pro-tumor microenvironment, thereby amplifying mutation-induced drug resistance by increasing the survival rate of tumor cells, a pattern consistent with our earlier results (Fig. 6b–c). Additionally, we scrutinized the evolution and distribution of phenotypes across different vessel-tumor distances (Fig. E.5). The outcomes reaffirmed the growth advantage of phenotype II over other mutated phenotypes. Collectively, these findings illustrate the synergistic acceleration of tumor drug resistance facilitated by the interplay between the vascular microenvironment and gene mutations.

3.5. Verification using clinical data

Based on our simulation findings, which indicate that both genetic mutations and angiogenesis contribute to drug resistance in GBM tumors, we hypothesized that GBM patients with more mutated genes or closer vessel-tumor distances would exhibit reduced sensitivity to targeted therapies and consequently experience poorer prognoses. To validate our model's predictions, we assembled a dataset comprising single-cell RNA-seq, bulk RNA-seq, spatial transcriptomics, somatic mutation, and clinical data from GBM patients who underwent targeted therapies, and we conducted K-M survival analysis.

The K-M survival analysis for gene mutation numbers in glioma patients (Fig. 8a) showed that individuals with a greater number of mutated genes had shorter PFS time. This is consistent with our model's predictions that the accumulation of genetic mutations in tumors with earlier mutations leads to larger tumor cell populations (Fig. 4). Furthermore, the K-M survival analysis for vessel-tumor distance for glioma patients (Fig. 8b) indicates that GBM patients with smaller vessel-tumor distance had lower PFS rate. This is in harmony with our simulations which indicated that closer vessel-tumor distance is more conducive to tumor progression during drug treatment (Fig. 6).

To validate the combined prognostic impact of gene mutations and vessel-tumor distance, we employed multivariable Cox regression analysis to calculate a risk score for each patient based on the number of gene mutations and vessel-tumor distance. The analysis reveals that patients with a close vessel-tumor distance or a higher number of gene mutations exhibited elevated risk scores. Subsequently, the K-M survival analysis based on these risk scores (Fig. 8c) indicated that the high-risk score group had a lower PFS rate. This corresponds with our predictions that tumors characterized by a closer vessel-tumor distance and an increased number of genetic mutations are more resistant to targeted therapies (Fig. 7a). Moreover, we found that the log-rank test *p*-value for these two variables (i.e., genetic mutations and vessel-tumor distance)

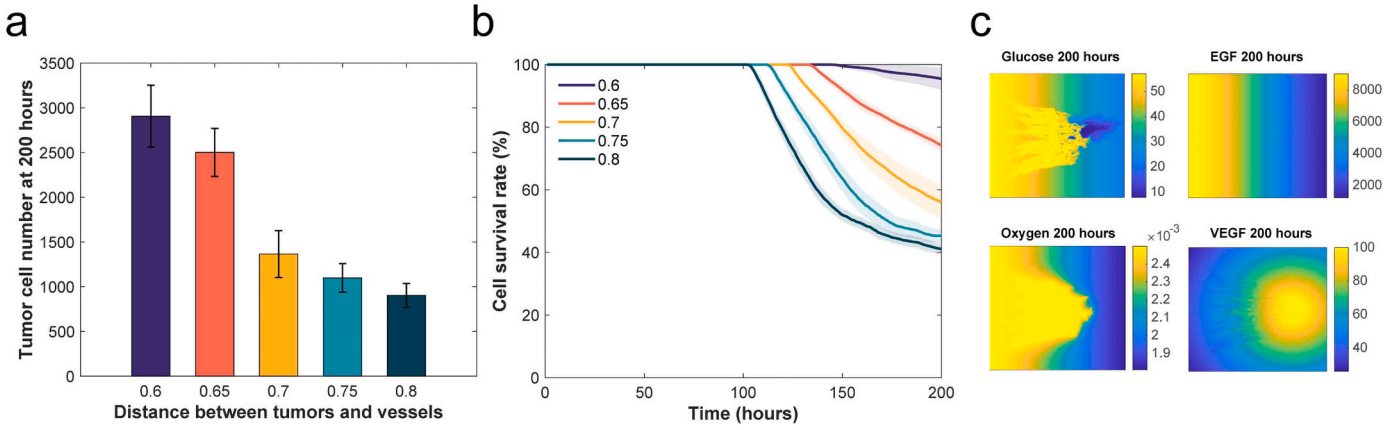

Fig. 6. Effect of the distance between blood vessels and tumors on the tumor growth during drug treatment. Five values (0.6, 0.65, 0.7, 0.75, and 0.8) representing the distance between the parent blood vessel and the tumor's center (V-T distance) were investigated. (a) The number of tumor cells at the 200-hour mark for the five different scenarios of V-T distances, based on data from 10 simulations. (b) Time-dependent survival rate curves for the five V-T distance scenarios. The solid lines represent the mean values, and the shaded areas indicate the 95% confidence interval. (c) Spatial distributions of four microenvironmental factors (glucose, oxygen, EGF, and VEGF) for a V-T distance of 0.6.

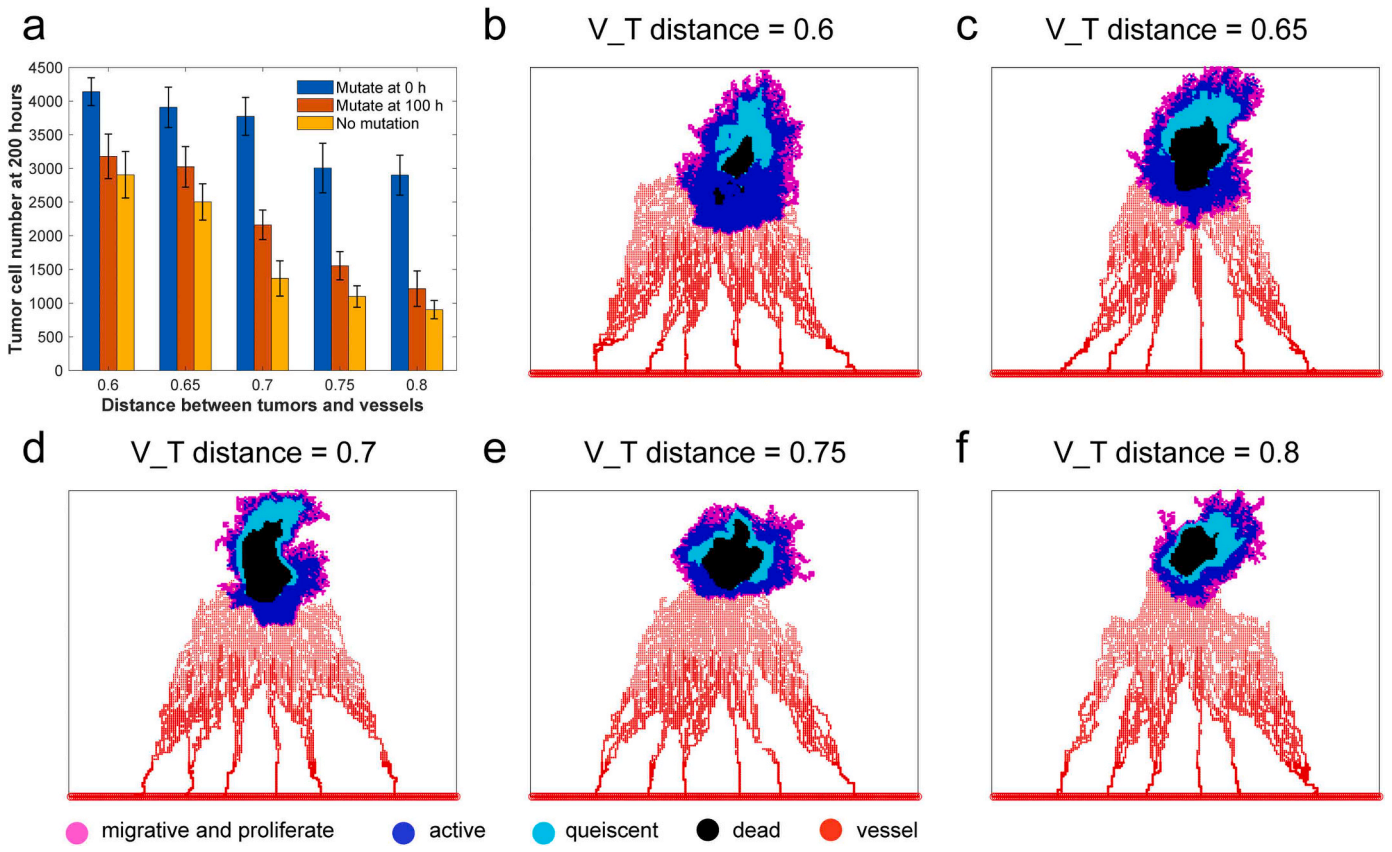

Fig. 7. Effect of the vessel-tumor distance on mutation-induced drug resistance. Five distinct values (0.6, 0.65, 0.7, 0.75, and 0.8) representing the vessel-tumor distance (V-T distance) were examined, alongside two mutation time points (mutation initiation at 0 h or 100 h). (a) The tumor cell population at the 200-hour mark across the various V-T distances and mutation time points, based on data from 10 simulations. (b–f) Spatial patterns of vascular tumor growth (assessed at 200 h), corresponding to gene mutations commencing at 0 h, with V-T distances set at 0.6 (b), 0.65 (c), 0.7 (d), 0.75 (e), and 0.8 (f).

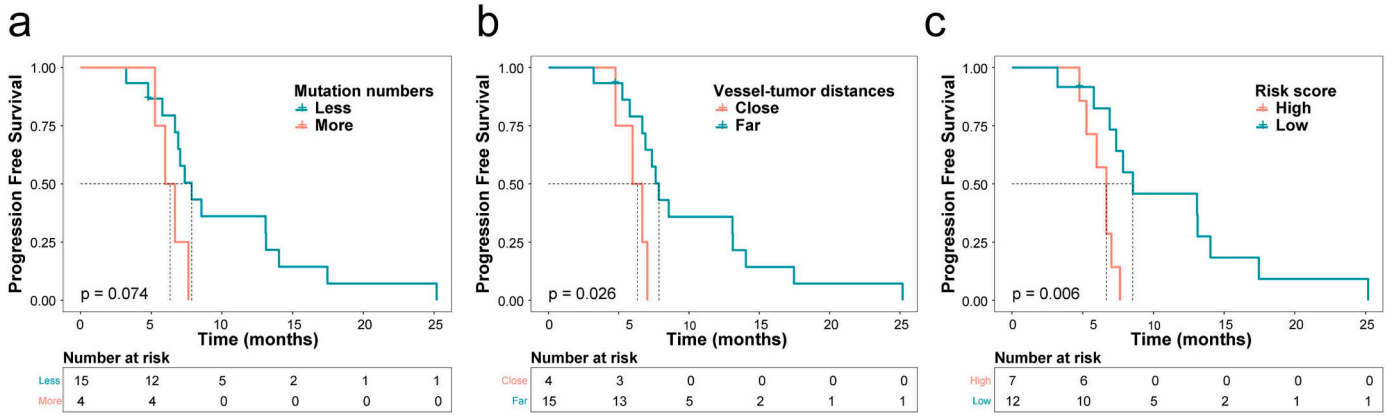

Fig. 8. Individual and combined prognostic effect of gene mutation numbers and vessel-tumor distance for glioma patients. (a) K-M survival analysis of the number of gene mutations. (b) K-M survival analysis of vessel-tumor distance. (c) K-M survival analysis of gene mutation numbers and vessel-tumor distance.

($p = 0.006$, Fig. 8c) was lower than that for each individual variable ($p = 0.074$, Fig. 8a; $p = 0.026$, Fig. 8b). This suggests that the combined variables enhanced the prognostic significance in comparison to each individual variable, further validating the synergistic combination effect of the vascular microenvironment and gene mutations on tumor drug resistance.

4. Discussion

Over the past decades, many mathematical models have been developed to simulate tumor evolution, such as ODE models [29,30], stochastic differential equation models [31–33], partial differential equation models [34,35], agent-based models [36,37], and hybrid models [38,39]. These models have shed light on the biological mechanisms underlying tumor growth, offering valuable insights into the intricacies of drug resistance.

However, to date, there has been a scarcity of mathematical models that comprehensively integrate both gene mutations and angiogenesis, despite their well-established significance in cancer progression, extensively explored through experimental studies. In our investigation,

we have developed a multiscale model that incorporates an agent-based representation of cellular phenotypes, ODEs of signaling pathways, stochastic simulations of gene mutations, the spatial–temporal evolutions of microenvironmental factors, and a rule-based portrayal of angiogenesis. This innovative model served as our tool to scrutinize the combined influences of genetic mutations and angiogenesis on the spatial–temporal dynamics of tumor growth in response to TKI treatment.

To incorporate gene mutations into our agent-based tumor growth model, we introduced a connection between gene mutations and alterations in the migration and proliferation capabilities of tumor cells. This was achieved by introducing random adjustments to the threshold parameters governing migration and proliferation. As such, several mutant phenotypes of tumor cells, each characterized by distinct thresholds, emerged during the simulations.

Initially, drug treatment exhibited effectiveness in restraining tumor growth. However, a marked expansion of tumors ensued after the occurrence of mutations, with the timing of mutations exerting influence, as earlier mutations led to more extensive tumor proliferation. This phenomenon can be attributed to tumors with earlier mutations accumulating a greater number of mutated genes, thereby elevating their propensity for progression, as supported by the K-M survival analysis concerning genetic mutation numbers. Furthermore, among the mutant phenotypes, the one with the most robust migration capacity predominated within the tumor population and tended to localize in the outer tumor layer. We speculate that mutations augment the heterogeneity among tumor cells, enhancing their adaptability to the dynamic and challenging growth environment. Besides, cell growth is inextricably tied to the availability of living space and nutrient concentrations. Therefore, mutant phenotypes with stronger migration abilities were more inclined to occupy advantageous positions for reproduction.

In addition to gene mutations, we also investigated the impact of the vascular microenvironment on tumor growth and drug resistance. We specifically examined how the distance between the tumor and the parent blood vessels impacted tumor expansion and treatment outcomes. The results showed that tumors situated in closer proximity to blood vessels exhibited accelerated growth rates and diminished survival rates. This can be reasonably interpreted as follows: the vascular microenvironment provides the tumor with an ample supply of nutrients and growth factors, fortifying their resilience against drug interventions and sustaining their vitality. Furthermore, we subjected our results to validation through K-M survival analysis.

In fact, both gene mutations and angiogenesis have been demonstrated as indispensable factors in tumor progression, leading to numerous excellent studies exploring drug resistance mechanisms from these two perspectives. For instance, mathematical models for the interconversion of phenotypes (sensitive and resistant) in GBM [40,41] have been developed, revealing that mutations induce tumor evolution towards a more adaptive resistant environment, aligning with our findings. In contrast to most previous studies that categorized tumor cells into sensitive and resistant phenotypes, we consider that post-mutation cell phenotypes should exhibit greater diversity and randomness. Therefore, we introduce a broader range of mutated phenotypes to investigate potential behaviors that may contribute to tumor resistance. Furthermore, many scholars have shown a keen interest in the role of blood vessels in tumor progression. For instance, a hybrid cellular automaton model was developed to assess how different vascular distributions affect tumor treatment outcomes [42]. They also acknowledged the role of blood vessels in promoting tumor resistance. However, they only viewed blood vessels as mere nutrient transporters, neglecting the feedback loop from tumor cells to the vasculature. In contrast, our model takes into account the interplay between blood vessels, tumors, and the microenvironment, aligning more closely with the realistic dynamics of tumor growth. Another study [43] demonstrated the mutual dependence of tumors and blood vessels, further validating our modeling framework. Collectively, these previous studies consistently support our conclusion on the roles of mutations and angiogenesis during tumor growth and drug response. However, these studies have remained at a single level, whereas our model integrates both intracellular and extracellular influencing factors. By coupling molecular, cellular, and microenvironmental levels, our model not only describes tumor growth and drug resistance processes but also explores the roles played by mutations and angiogenesis in this process.

The model developed in this study offers a valuable framework for integrating multiple levels of biological mechanisms within a dynamic system. In particular, the model incorporates gene mutations and angiogenesis to elucidate their influences on tumor growth and drug resistance. However, we acknowledge certain limitations in our model. Firstly, akin to other models, our framework simplifies the intricate biological processes despite its incorporation of multiple scales and multi-dimensional variables. There are over 50 different growth factors that act on over 50 receptor tyrosine kinases, forming a complex signaling unit. However, our model only incorporates six microenvironmental factors, i.e., glucose, oxygen, fibronectin, EGF, VEGF, and drug, as representative variables for simulation. As tumor microenvironment and signaling mechanisms are complicated, we used EGF as a representative growth factor in the tumor microenvironment and a classical EGFR pathway as a representative oncogenic signaling pathway. As for VEGF signaling pathway, it is complex and the mechanisms by which VEGF determines the proliferation and migration of endothelial cells are not fully clear to us. Moreover, it is hard to quantify the VEGF signaling pathway due to the lack of enough experimental data for the biochemical reactions involved in this pathway. To avoid introducing additional uncertainty into our model, we did not include VEGF into the current model. Nevertheless, it's valuable to model VEGF signaling pathway and incorporate it into the multiscale model of tumor growth in the future studies.

Secondly, our model falls short of integrating high-throughput biological data from diverse scales. The advent and progression of single-cell and spatially resolved omics data (e.g., single-cell RNA-seq, single-cell proteomics, single-cell metabolomics, and spatial transcriptomics data), now facilitate the development of data-informed, single cell-based multiscale models [44]. For example, single-cell or spatial transcriptomics data can quantitatively delineate cell-to-cell communication networks [45–47] or signaling networks [48,49]. Such data can be incorporated into our multiscale modeling approach to account for the complex signaling mechanisms underlying a broader array of growth factors and receptor tyrosine kinases, as mentioned earlier.

In summary, this study developed a multiscale model to investigate the evolutionary dynamics of vascular tumor growth in the presence of mutations. Our model revealed that both intrinsic genetic mutations and extrinsic microenvironmental adaptations influence the spatial–temporal dynamics of tumor growth in response to TKI treatment. This research contributes to our comprehension of drug resistance mechanisms and potential treatment strategies.

CRediT authorship contribution statement

Heng Yang: Methodology, Software, Validation, Formal analysis, Visualization, Writing - Original Draft. **Haofeng Lin**: Software, Investigation. **Xiaoqiang Sun**: Conceptualization, Methodology, Validation, Writing- Reviewing and Editing, Supervision, Funding acquisition.

Declaration of Competing Interest

The authors declare that they have no known competing financial interests or personal relationships that could have appeared to influence the work reported in this paper.

Acknowledgments

XS was supported by grants from the National Natural Science

Foundation of China (62273364 and 11871070), the Guangdong Basic and Applied Basic Research Foundation (2020B1515020047), and the Fundamental Research Funds for the Central Universities, Sun Yat-sen University (231lgbj025).

Appendix A. Supporting information

Supplementary data associated with this article can be found in the online version at doi:10.1016/j.csbj.2023.10.037.

References

[1] Louis DN, Perry A, Reifenberger G, von Deimling A, Figarella-Branger D, Cavenee WK, et al. The 2016 World Health Organization classification of tumors of the central nervous system: a summary. Acta Neuropathol 2016;131(6):803–20.
[2] Comprehensive genomic characterization defines human glioblastoma genes and core pathways. Nature 2008;455(7216):1061–8.
[3] Qin A, Musket A, Musich PR, Schweitzer JB, Xie Q. Receptor tyrosine kinases as druggable targets in glioblastoma: do signaling pathways matter? Neuro-Oncol Adv 2021;3(1).
[4] Dean M, Fojo T, Bates S. Tumour stem cells and drug resistance. Nat Rev Cancer 2005;5(4):275–84.
[5] Brown R, Curry E, Magnani L, Wilhelm-Benartzi CS, Borley J. Poised epigenetic states and acquired drug resistance in cancer. Nat Rev Cancer 2014;14(11):747–53.
[6] Quail DF, Bowman RL, Akkari L, Quick ML, Schuhmacher AJ, Huse JT, et al. The tumor microenvironment underlies acquired resistance to CSF-1R inhibition in gliomas. Science 2016;352(6288):aad3018.
[7] Meads MB, Gatenby RA, Dalton WS. Environment-mediated drug resistance: a major contributor to minimal residual disease. Nat Rev Cancer 2009;9(9):665–74.
[8] Obenauf AC, Zou Y, Ji AL, Vanharanta S, Shu W, Shi H, et al. Therapy-induced tumour secretomes promote resistance and tumour progression. Nature 2015;520 (7547):368–72.
[9] Quail DF, Joyce JA. The microenvironmental landscape of brain tumors. Cancer Cell 2017;31(3):326–41.
[10] Barker HE, Paget JT, Khan AA, Harrington KJ. The tumour microenvironment after radiotherapy: mechanisms of resistance and recurrence. Nat Rev Cancer 2015;15 (7):409–25.
[11] Goldie JH, Coldman AJ. A mathematic model for relating the drug sensitivity of tumors to their spontaneous mutation rate. Cancer Treat Rep 1979;63(11–12): 1727.
[12] Panetta JC. A mathematical model of drug resistance: heterogeneous tumors. Math Biosci 1998;147(1):41–61.
[13] Foo J, Michor F. Evolution of resistance to targeted anti-cancer therapies during continuous and pulsed administration strategies. PLoS Comput Biol 2009;5(11): e1000557.
[14] Pisco AO, Brock A, Zhou J, Moor A, Mojtahedi M, Jackson D, et al. Non-Darwinian dynamics in therapy-induced cancer drug resistance. Nat Commun 2013;4(9): 2467.
[15] Bozic I, Nowak MA. Timing and heterogeneity of mutations associated with drug resistance in metastatic cancers. Proc Natl Acad Sci USA 2014;111(45):15964–8.
[16] Fu F, Nowak MA, Bonhoeffer S. Spatial heterogeneity in drug concentrations can facilitate the emergence of resistance to cancer therapy. PLoS Comput Biol 2015;11 (3):e1004142.
[17] Sun X, Zhang L, Tan H, Bao J, Strouthos C, Zhou XJBb. Multi-scale agent-based brain cancer modeling and prediction of TKI treatment response: incorporating EGFR signaling pathway and angiogenesis 2012;13(1):1–14.
[18] Liang W, Zheng Y, Zhang J, Sun X. Multiscale modeling reveals angiogenesis-induced drug resistance in brain tumors and predicts a synergistic drug combination targeting EGFR and VEGFR pathways. BMC Bioinforma 2019;20 (Suppl 7):203.
[19] Pérez-Gutiérrez L, Ferrara N. Biology and therapeutic targeting of vascular endothelial growth factor A. Nat Rev Mol Cell Biol 2023.
[20] Schlessinger J, Ullrich A. Growth factor signaling by receptor tyrosine kinases. Neuron 1992;9(3):383–91.
[21] Kholodenko BN, Demin OV, Moehren G, Hoek JB. Quantification of short term signaling by the epidermal growth factor receptor*. J Biol Chem 1999;274(42): 30169–81.
[22] Mansury Y, Deisboeck TS. The impact of "search precision" in an agent-based tumor model. J Theor Biol 2003;224(3):325–37.
[23] Sun X, Liu X, Xia M, Shao Y, Zhang XD. Multicellular gene network analysis identifies a macrophage-related gene signature predictive of therapeutic response and prognosis of gliomas. J Transl Med 2019;17(1):159.
[24] Liao J, Qian J, Fang Y, Chen Z, Zhuang X, Zhang N, et al. De novo analysis of bulk RNA-seq data at spatially resolved single-cell resolution. Nat Commun 2022;13(1): 6498.
[25] Abdelfattah N, Kumar P, Wang C, Leu JS, Flynn WF, Gao R, et al. Single-cell analysis of human glioma and immune cells identifies S100A4 as an immunotherapy target. Nat Commun 2022;13(1):767.
[26] Ravi VM, Will P, Kueckelhaus J, Sun N, Joseph K, Salie H, et al. Spatially resolved multi-omics deciphers bidirectional tumor-host interdependence in glioblastoma. Cancer Cell 2022;40(6):639–55. e13.
[27] Jászai J, Schmidt MHJC. Trends and challenges in tumor anti-angiogenic therapies 2019;8(9):1102.
[28] Pretzsch E, Bösch F, Neumann J, Ganschow P, Bazhin A, Guba M, et al. Mechanisms of metastasis in colorectal cancer and metastatic organotropism: hematogenous versus peritoneal spread 2019;2019.
[29] Wei HC. Mathematical modeling of tumor growth: the MCF-7 breast cancer cell line. Math Biosci Eng 2019;16(6):6512–35.
[30] Tomasetti C, Levy D. An elementary approach to modeling drug resistance in cancer. Math Biosci Eng 2010;7(4):905–18.
[31] Sun X, Bao J, Shao Y. Mathematical modeling of therapy-induced cancer drug resistance: connecting cancer mechanisms to population survival rates. Sci Rep 2016;6(1):22498.
[32] Tanaka G, Hirata Y, Goldenberg SL, Bruchovsky N, Aihara K. Mathematical modelling of prostate cancer growth and its application to hormone therapy. Philos Trans A Math Phys Eng Sci 2010;368(1930):5029–44.
[33] Lindsay D, Garvey CM, Mumenthaler SM, Foo J. Leveraging hypoxia-activated prodrugs to prevent drug resistance in solid tumors. PLoS Comput Biol 2016;12(8): e1005077.
[34] Zheng Y, Bao J, Zhao Q, Zhou T, Sun X. A spatio-temporal model of macrophage-mediated drug resistance in glioma immunotherapy. Mol Cancer Ther 2018;17(4): 814–24.
[35] Li S, Wang S, Zou X. Data-driven mathematical modeling and quantitative analysis of cell dynamics in the tumor microenvironment. Comput Math Appl 2022;113: 300–14.
[36] Schneckenreither G, Tschandl P, Rippinger C, Sinz C, Brunmeir D, Popper N, et al. Reproduction of patterns in melanocytic proliferations by agent-based simulation and geometric modeling. PLoS Comput Biol 2021;17(2):e1008660.
[37] Storey KM, Jackson TL. An agent-based model of combination oncolytic viral therapy and Anti-PD-1 immunotherapy reveals the importance of spatial location when treating glioblastoma. Cancers (Basel) 2021;13(21):5314.
[38] Jafari Nivlouei S, Soltani M, Carvalho J, Travasso R, Salimpour MR, Shirani E. Multiscale modeling of tumor growth and angiogenesis: Evaluation of tumor-targeted therapy. PLoS Comput Biol 2021;17(6):e1009081.
[39] Anderson AR. A hybrid mathematical model of solid tumour invasion: the importance of cell adhesion. Math Med Biol 2005;22(2):163–86.
[40] Trobia J, Tian K, Batista AM, Grebogi C, Ren HP, Santos MS, et al. Mathematical model of brain tumour growth with drug resistance. Commun Nonlinear Sci 2021; 103:106013.
[41] Hanum L., Susyanto N., Ertiningsih D. Mathematical Model of the Impact of Chemotherapy and Anti-Angiogenic Therapy on Drug Resistance in Glioma Growth. arXiv preprint 2023.
[42] Scott JG, Fletcher AG, Anderson AR, Maini PK. Spatial metrics of tumour vascular organisation predict radiation efficacy in a computational model. PLoS Comput Biol 2016;12(1):e1004712.
[43] Voutouri C, Kirkpatrick ND, Chung E, Mpekris F, Baish JW, Munn LL, et al. Experimental and computational analyses reveal dynamics of tumor vessel cooption and optimal treatment strategies. P Natl Acad Sci USA 2019;116(7): 2662–71.
[44] Cang Z, Wang Y, Wang Q, Cho KWY, Holmes W, Nie Q. A multiscale model via single-cell transcriptomics reveals robust patterning mechanisms during early mammalian embryo development. PLoS Comput Biol 2021;17(3):e1008571.
[45] Zhang J, Guan M, Wang Q, Zhang J, Zhou T, Sun X. Single-cell transcriptome-based multilayer network biomarker for predicting prognosis and therapeutic response of gliomas. Brief Bioinforma 2020;21(3):1080–97.
[46] Cheng J, Zhang J, Wu Z, Sun X. Inferring microenvironmental regulation of gene expression from single-cell RNA sequencing data using scMLnet with an application to COVID-19. Brief Bioinforma 2021;22(2):988–1005.
[47] Ni X, Wu W, Sun X, Ma J, Yu Z, He X, et al. Interrogating glioma-M2 macrophage interactions identifies Gal-9/Tim-3 as a viable target against PTEN-null glioblastoma. Sci Adv 2022;8(27):eabl5165.
[48] Sun X, Zhang J, Nie Q. Inferring latent temporal progression and regulatory networks from cross-sectional transcriptomic data of cancer samples. PLoS Comput Biol 2021;17(3):e1008379.
[49] Dong Z, Sun X. Inferring disease progression and gene regulatory networks from clinical transcriptomic data using PROB_R. STAR Protoc 2022;3(3):101467.